

Article

# Biomass-Based Cellulose Functionalized by Phosphonic Acid with High Selectivity and Capacity for Capturing U(VI) in Aqueous Solution

Zhipeng Huo <sup>1,\*</sup> , Sheng Zhao <sup>1,2</sup>, Jinxin Yi <sup>1,2</sup>, Hong Zhang <sup>1</sup> and Jiaying Li <sup>1,\*</sup> 

<sup>1</sup> Institute of Plasma Physics, Hefei Institutes of Physical Science, Chinese Academy of Sciences, Hefei 230031, China; zs321@mail.ustc.edu.cn (S.Z.); yjxy@mail.ustc.edu.cn (J.Y.); hong.zhang@ipp.ac.cn (H.Z.)

<sup>2</sup> Science Island Branch of Graduate School, University of Science and Technology of China, Hefei 230031, China

\* Correspondence: zhipeng.hu@ipp.ac.cn (Z.H.); lijx@ipp.ac.cn (J.L.)

Received: 10 July 2020; Accepted: 30 July 2020; Published: 7 August 2020



**Abstract:** Uranium could be released into the aquatic ecological environment through various sorts of nuclear-related procedures, which has high toxicity and carcinogenicity even with a trace amount. A novel phosphonic acid functionalized cellulose adsorbent (PVKAP) with a simple synthesis strategy is developed based on pumpkin vine cellulose (PVK) as the substrate material for efficient and selective capturing U(VI). Because of the strong coordination between phosphonic acid groups and U(VI), the adsorption efficiency and adsorption selectivity of modified cellulose to U(VI) are greatly improved. The adsorption behavior follows the Langmuir adsorption model and pseudo-second-order kinetics model. The maximum adsorption capacities (pH = 5,  $T = 293$  K) of PVK and PVKAP obtained from Langmuir isotherm are 57.2 and 714.3 mg g<sup>-1</sup>, and the adsorption equilibrium are reached in 240 and 35 min, respectively. Additionally, PVKAP has a high adsorption selectivity which reached 70.36% for U(VI) in multi-ion condition, and recycling studies have shown that PVKAP has good recyclability. Furthermore, batch adsorption experiments and spectral analysis reveal that the efficient enrichment of U(VI) on PVKAP could mainly attribute to the inner layer complexation. Therefore, this environmentally friendly and simple route prepared PVKAP has good a potential application value for U(VI) enrichment in aqueous media related to nuclear waste.

**Keywords:** phosphonic acid; cellulose; U(VI); adsorption selectivity; biomass

## 1. Introduction

Uranium, as an important resource of nuclear fuel [1], could be released into the aquatic ecological environment through various sorts of nuclear-related procedures including waste treatment, spent fuel reprocessing, nuclear accidents, and so on [2–5]. Uranium primarily exists in the form of uranyl (UO<sub>2</sub><sup>2+</sup>) ion with good solubility and fluidity [6,7] at pH ≤ 5, which has high toxicity and carcinogenicity even with trace amounts and has an exceedingly long half-life of ~10<sup>8</sup> years [2,8–10]. Therefore, there is an urgent need to develop functional materials to capture U(VI) from radioactive water. Adsorption methods, as diffusely utilized wastewater treatment approaches, have received much attention due to their excellent removal performance, high availability and ease of operation [11–15]. So far, various materials have been exploited for removal of U(VI), such as metal organic frameworks (MOF) [16–19], functionalized mesoporous silica [20–22], carbon-based nanomaterials [23–26], and natural polymers [24,27]. In general, superior adsorbents should meet the combined requirements of high adsorption capacity, ultra-fast removal rate, high selectivity, stability, and recyclability. However, few of the adsorption materials mentioned above could cover all these

characteristics. Importantly, the adsorption selectivity of U(VI) is a significant characteristic, due to the co-existing metal ions in the wastewater that could also compete with U(VI) on the adsorption sites of the adsorbents [4,20,28,29]. Furthermore, the conventional preparation of U(VI) adsorbents is multiplex, costly, and not eco-friendly. Therefore, it is highly imperative to exploit a facile strategy to fabricate efficient adsorbents for U(VI) with high selectivity.

Cellulose, as the most abundant natural polymer, could be obtained from various natural resources including plants, woods, and so on. Because of its exceptional characteristics such as environmentally friendly, biodegradability, and low cost, it can be employed as adsorbents [30–32]. Moreover, cellulose has an abundance of hydroxyl groups [33–35], which could be modified with functional groups such as sulpho groups, carboxyl groups, and amino groups [36–38]. Pumpkin planting is very common and there is abundant waste pumpkin vine in rural China, which is an abundant feedstock to derived cellulose. In this research, in view of the above environmental requirements, a reasonable synthetic strategy is developed to fabricate a novel phosphonic acid and acrylic acid functionalized pumpkin vine based cellulose adsorbent (PVKAP) for efficient elimination of U(VI) with high selectivity. Owing to the strong complexation between phosphonate sites (P=O) in the polymeric matrix and U(VI) [39], the PVKAP probably shows excellent selectivity and high removal performance to U(VI). Therefore, a series of characterizations are carried out to analyze the physico-chemical characteristics of pumpkin vine cellulose (PVK) and PVKAP. Batch experiments and ICP-AES are adopted to explore the adsorption behavior and selectivity of PVK and PVKAP to uranium under different conditions. Furthermore, the potential adsorption mechanism was, in detail, revealed by FTIR and XPS techniques. This work demonstrates a novel and important strategy to obtain excellent adsorbents with high selectivity and capacity for capturing U(VI) in aqueous solution.

## 2. Experimental Part

### 2.1. Material Preparation

Pumpkin vine was obtained from Hefei, China. Acrylic acid (AA), Vinyl phosphate (VPA) and azobisisobutyronitrile (AIBN) were purchased from Sinopharm Chemical Reagent Co., Ltd. without further purification.  $\text{UO}_2(\text{NO}_3)_2 \cdot 6\text{H}_2\text{O}$  (purity of 99.99%) was bought from Sigma Aldrich. The uranium stock solution was prepared by dissolving  $\text{UO}_2(\text{NO}_3)_2 \cdot 6\text{H}_2\text{O}$  in Milli-Q water.

The functionalized pumpkin vine based cellulose adsorbent (PVKAP) was prepared by graft copolymerization of pumpkin vine-based cellulose under solvothermal conditions. The schematic of the synthetic route of PVKAP is shown in Figure S1 in the Supplementary Materials. The pumpkin vine was washed by Milli-Q water and then dried in a vacuum oven, then crushed into powder followed by washing by Milli-Q water and then dried in a vacuum oven. In total, 5 g of pumpkin vine powder was added into a three-necked and round-bottomed glass flask and mixed with 200 mL KOH solution ( $7\text{ mol L}^{-1}$ ), and reacted under the oil bath at  $70\text{ }^\circ\text{C}$  for 2 h with magnetically stir. Then, the suspension was filtered and repeatedly washed by Milli-Q water and then dried in vacuum oven at  $60\text{ }^\circ\text{C}$  for 12 h, and the product was designated as PVK. 2 g PVK was dispersed into 15 mL ethyl acetate to prepare a suspension solution, followed by adding 0.05 g AIBN under stirring for 15 min. Then vinyl phosphate (1.5 g) and acrylic acid (1.5 g) were added into the above-mentioned reaction mixture, and the mixture was transferred into a Teflon lining autoclave and reacted at  $100\text{ }^\circ\text{C}$  for 24 h. After the reaction completed and cooled to ambient temperature, the product was repeatedly washed thoroughly with Milli-Q water and ethanol. Finally, the product was freeze dried at  $-60\text{ }^\circ\text{C}$  for 12 h in a vacuum freeze dryer, and the product was designated as PVKAP.

### 2.2. Characterizations

The nanostructures and morphologies of PVK and PVKAP were performed on a JEOL JSM-7001F scanning electron microscope (SEM) with an accelerating voltage of 200 kV. The X-ray diffraction (XRD) patterns were recorded on a Philips X'Pert Pro Super diffractometer with  $\text{Cu K}\alpha$  radiation. The Fourier

transform infrared spectra (FT-IR) of the prepared materials were measured by a Nicolet-5700 FT-IR spectrophotometer. Brunauer–Emmett–Teller (BET) specific surface area analysis was carried out by nitrogen adsorption–desorption measurements at 77 K using a Quantachrom Autosorb IQ-C gas adsorption system. The thermogravimetric analysis (TGA) curves within 30–800 °C were calculated by a TGA-50/50H analyzer. The X-ray photoelectron spectroscopy (XPS) analyses were performed on a VG Scientific ESCALAB Mark II spectrometer. And the Figure S2 in the Supplementary Materials shows the original data for XPS experiments.

### 2.3. Adsorption Tests

A certain amount of sorbent suspension, uranium stock solution, NaNO<sub>3</sub>, and a multi-ion solution were simultaneously placed into a group of 10.0 mL PE tubes to attain the desired concentrations. Experimental equilibrium adsorption data of PVK and PVKAP were obtained under the condition of  $C_{U(VI)initial} = 12.8\sim 79.4 \text{ mg L}^{-1}$ ,  $m/V = 0.1 \text{ g L}^{-1}$ ,  $\text{pH} = 5$ . The pH values of the suspension were adjusted by adding a negligible volume of NaOH or HNO<sub>3</sub> solutions ( $0.1\text{--}1.0 \text{ mol L}^{-1}$ ) and measured by a pH meter. Then, the suspensions were oscillated in the reciprocating shaker for a specific time and temperature, and each PE tube was centrifuged to separate the solid phase from the liquid phase. The concentrations of U(VI) in the supernatants were determined by a kinetic phosphorescence analyzer (KPA-11, Richland, WA, USA). The concentrations of U(VI) mixed with other competitive absorption metal cations were measured by an inductively coupled plasma atomic emission spectroscopy (ICP-AES, Optima 7300 DV, Perkinelmer, Waltham, MA, USA). The adsorption capacities ( $q_e$ ) of U(VI) and adsorption percentage ( $R\%$ ) were calculated by the following equations [40]:

$$q_e = \frac{(C_0 - C_e) V}{m} \quad (1)$$

$$R\% = \frac{C_0 - C_e}{C_0} \times 100\% \quad (2)$$

where  $C_0$ ,  $C_e$ ,  $V$  and  $m$  represent the initial concentration of U(VI), the residual concentration of U(VI), the volume of uptake systems, and the mass of adsorbent, respectively. (In this work,  $C_0 = 0.5 \text{ mmol L}^{-1}$  for all cations,  $\text{pH} = 5.0 \pm 0.1$ ,  $m/V = 0.05 \text{ g L}^{-1}$ ). The adsorption selectivity related to U(VI) ( $S_U$ ) was measured to illustrate the effectiveness of selectivity of the adsorbent to U(VI):

$$S_U = \frac{q_e - U}{q_e - tol} \times 100\% \quad (3)$$

where  $q_{e-U}$  and  $q_{e-tol}$  are, respectively, the adsorbed amount of uranium and all cations in multi-ion solution.

### 2.4. Desorption and Regeneration Study

The desorption and regeneration of PVKAP were carried out for five consecutive cycles to evaluate the stability and reusability. In each cycle, the PVKAP loaded with U(VI) was centrifuged after saturation adsorption, followed by eluting it with HCl solution ( $0.1 \text{ mol L}^{-1}$ ) which was gently shaken in an oscillator at 293 K for 24 h, then repeatedly washed by ethanol and Milli-Q water and dried for recycling.

## 3. Results and Discussions

### 3.1. Structural Characterizations

The nanostructure and surface features of PVK and PVKAP were revealed by SEM shown in Figure 1. PVK and PVKAP are fibrous and both have a diameter of about 20–50  $\mu\text{m}$ . The PVK

(Figure 1a) exhibits a relatively smooth fibrous morphology, while the PVKAP (Figure 2a) shows a much rougher surface after grafting with VPA and AA, which is advantageous for trapping metal ions.

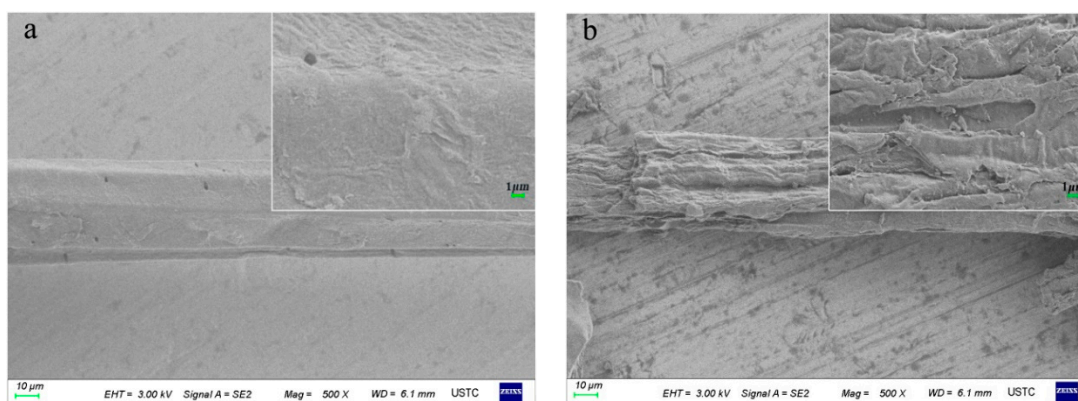


**Figure 1.** SEM images for pumpkin vine cellulose (PVK) (a) and a novel phosphonic acid and acrylic acid functionalized pumpkin vine based cellulose adsorbent (PVKAP) (b).

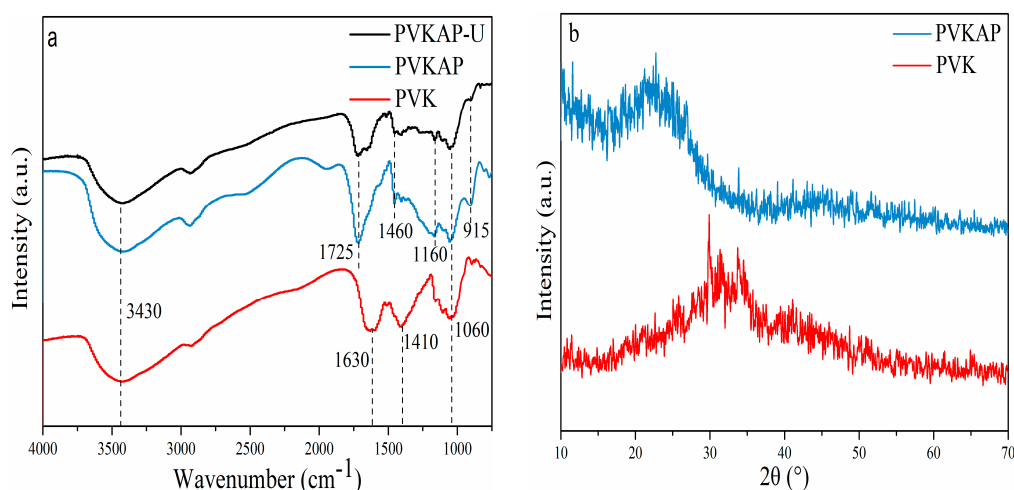


**Figure 2.** (a) FTIR spectra of PVK and PVKAP; (b) XRD patterns of PVK and PVKAP.

The functional groups on the surface of PVK and PVKAP were analyzed by FT-IR spectroscopy. As shown in Figure 2a, the characteristic absorption peaks of PVK at 3430, 1410, 1060, and 1630 cm<sup>-1</sup> are, respectively, attributed to the stretching vibration peaks of -OH, COO, and C-O, and the -OH bending vibration peak [39]. Comparing the FTIR spectra of PVKAP to PVK, the newly added peaks of PVKAP at 1725, 1460, 1160, and 915 cm<sup>-1</sup> are attributed to the stretching vibration peaks of C=O, P-C, P=O, and P-OH [41–43], respectively; thus, indicating that ethylene phosphate and acrylic acid were successfully grafted onto the surface of PVK by copolymerization. As confirmed by SEM, the FT-IR spectrum further demonstrates the successfully functionalized cellulose adsorbent materials. Furthermore, the P-OH characteristic vibration at 915 cm<sup>-1</sup> and the P=O characteristic vibration peak at 1160 cm<sup>-1</sup> almost disappeared, and the characteristic vibration of C=O at 1725 cm<sup>-1</sup> and the -OH characteristic vibration peak at 3430 cm<sup>-1</sup> weakened after the uranyl was absorbed by PVKAP (PVKAP-U); thus, indicating that the phosphonic acid group and the hydroxyl site participate in the capturing of U(VI) [39,44]. Simultaneously, the XRD pattern (Figure 2b) of PVKAP exhibits an added broad peak in the range of 15 to 30° compared to PVK, while the major diffraction peaks remain unchanged. This significantly broad diffraction peak of PVKAP may be attributed to the grafted polymer chain, which confirms successful copolymerization and is in line with the results of FTIR spectroscopy.

To further understand the specific surface area and pore size distribution of PVK and PVKAP, the BET method was adopted to analyze the samples. The N<sub>2</sub> adsorption–desorption adsorption isotherms of PVK and PVKAP are shown in Figure 3a. Furthermore, the specific surface area, pore volume and average pore size are shown in Table 1. Obviously, the specific surface area is improved after functionalization, and the average pore diameter of about 5 nm indicates the existence of internal mesopores. Additionally, the significant uptake of the nitrogen adsorption–desorption adsorption isotherm of PVKAP at relatively high pressures (0.8–1.0) also indicates the presence of mesopores [38,45].

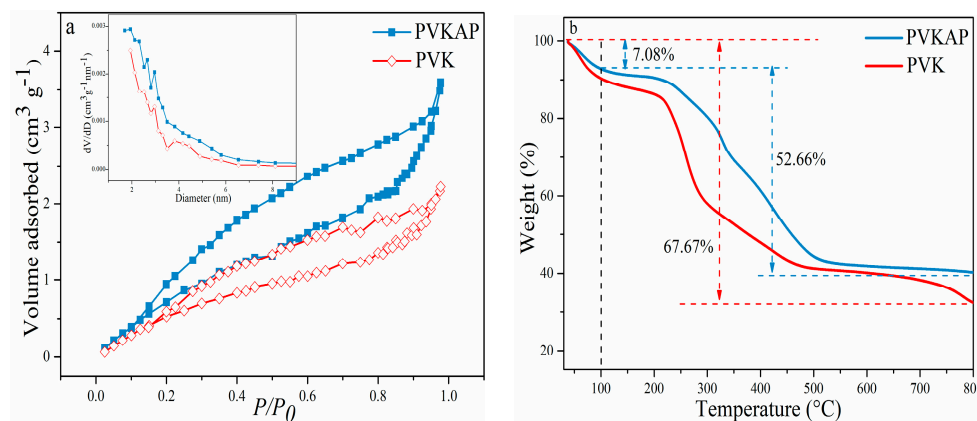


**Figure 3.** (a) Nitrogen adsorption–desorption isotherms of PVK and PVKAP; (b) the thermogravimetric analysis (TGA) analysis curves of PVK and PVKAP.

**Table 1.** Pore structure parameters of PVK and PVKAP.

Sample	BET Surface Area (m <sup>2</sup> g <sup>-1</sup> )	Pore Volume (cm <sup>3</sup> g <sup>-1</sup> )	Average Pore Size (nm)
PVK	5.02	4.954 × 10 <sup>-3</sup>	4.47
PVKAP	6.63	7.965 × 10 <sup>-3</sup>	5.12

Generally, radioactive wastewater under certain circumstances has a relatively high temperature due to the fission of radionuclides, so thermal stability is one of the significant physicochemical properties to value adsorbent performance. As shown in Figure 3b, the TGA curves of PVK and PVKAP exhibit similar characteristics, of which the weight loss processes can be divided into three stages. The first stage loses weight at about 100 °C, which corresponds to the dissipation of water molecules from the surfaces of the materials; the second stage loses weight at around 100–238 °C. The weight loss of PVK at this stage is mainly attributable to the consumption of hydroxyl sites. Meanwhile, the weight loss of PVKAP at this stage is less than PVK, which is ascribed to the consumption of hydroxyl groups and the grafted phosphonic acid groups and carboxyl groups [41,42]. In the third stage, the weight loss of PVK at 238–800 °C is mainly caused by the collapse of the cellulose skeleton at high temperature, and the disintegration rate of the skeleton is slowed down due to the polymer grafted on the surface of PVKAP. These above results confirm that the successful copolymerization of vinyl phosphate and acrylic acid are grafted onto the surface of PVK, and the graft ratio is about 7.93%. Therefore, the improved thermal stability of PVKAP is beneficial for its application to the purification of wastewater containing radionuclides under certain circumstances.

### 3.2. Adsorption Isotherms

The Langmuir adsorption model and Freundlich adsorption model were adopted to evaluate the adsorption capacity of PVK and PVKAP to U(VI). Further details about Langmuir and Freundlich isotherm adsorption models have been explained in the Supplementary Materials. Figure 4 and Table 2 show the specific fitting parameters, the adsorption capacity of U(VI) by PVKAP is significantly improved. Additionally, the adsorption capacity of PVKAP to U(VI) increases as the initial U(VI)

concentration increases, indicating that the initial U(VI) concentration is the main driving force for the liquid–solid phase adsorption. Furthermore, the capture capacity of PVKAP increases rapidly when the U(VI) concentration is relatively low, while the adsorption capacity increases slowly as its concentration increases to relatively high values. Thus, the efficient capture of U(VI) by PVKAP could be ascribed to surface complexation rather than U(VI) precipitation [46].

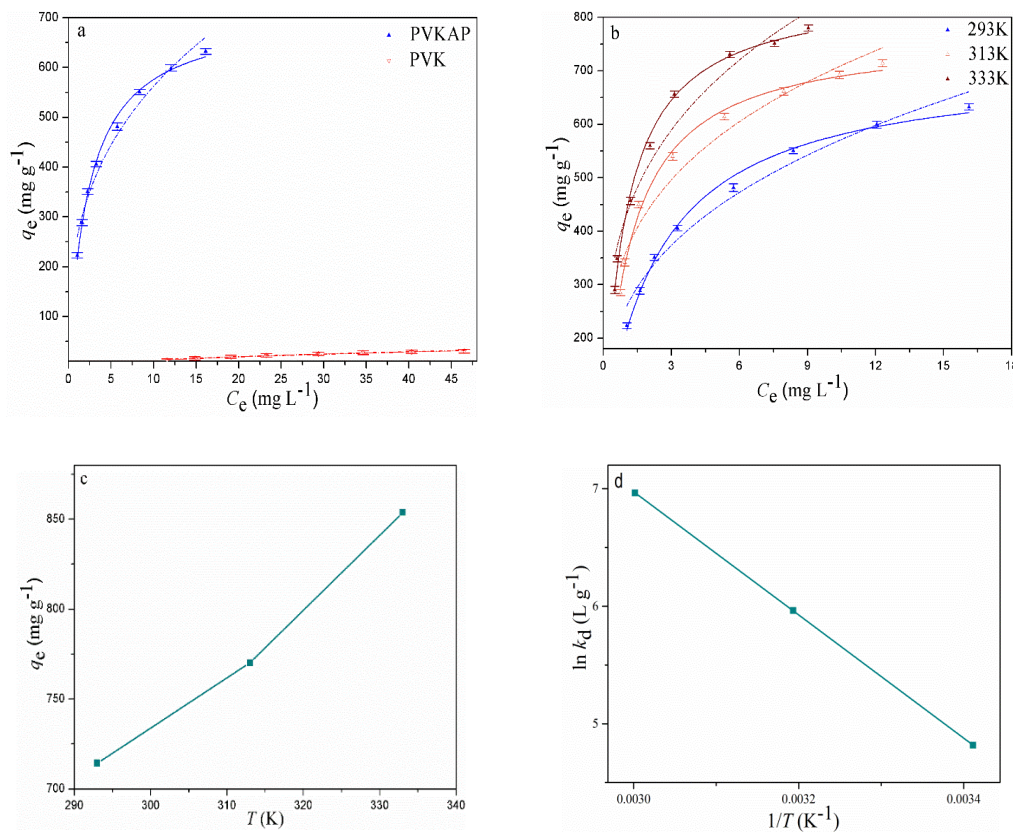


**Figure 4.** (a) Experimental equilibrium adsorption data of PVK and PVKAP under the condition of  $m/V = 0.1 \text{ g L}^{-1}$ ,  $C_{U(VI)initial} = 12.8\sim 79.4 \text{ mg L}^{-1}$ ,  $\text{pH} = 5$  and  $293 \text{ K}$ ; (b) adsorption isotherms of Langmuir (solid line) and Freundlich (dash line) for PVKAP capturing (VI) under different temperatures; (c) effect of temperature on the U (VI) captured by PVKAP; (d) variation of  $\ln K_d$  with  $T^{-1}$ .

**Table 2.** Isotherms parameters of Langmuir and Freundlich for PVK and PVKAP.

Adsorbate	$T$ (K)	$q_e$ (mg g <sup>-1</sup> )	Langmuir $K_L$ (L mg <sup>-1</sup> )	$R^2$	$K_F$ (mg <sup>1-n</sup> L <sup>n</sup> g <sup>-1</sup> )	Freundlich $n$	$R^2$
PVK	293	57.2	0.03	0.991	3.2	0.60	0.971
PVKAP	293	714.3	0.42	0.995	257.5	0.34	0.971
PVKAP	313	770.2	0.82	0.994	362.3	0.29	0.950
PVKAP	333	853.7	1.03	0.994	428.8	0.29	0.952

Simultaneously, the fitting results of the Langmuir adsorption model show that the maximum adsorption capacities ( $\text{pH} = 5$ ,  $T = 293 \text{ K}$ ) of PVK and PVKAP are  $57.2$  and  $714.3 \text{ mg g}^{-1}$ , respectively. The significantly increased adsorption capacity of PVKAP could be attributed to the increased adsorption sites introduced by copolymerization on the surface of PVK, which is in accord with the results of FTIR spectroscopy. In addition, the Langmuir adsorption model could be better to describe the adsorption process of U(VI) on PVKAP compared to the Freundlich adsorption model, which indicates that the active adsorption sites on PVKAP are uniformly distributed, and the adsorption process is a single layer adsorption process.

### 3.3. Adsorption Thermodynamics

The influence of temperature on the adsorption of U(VI) by PVKAP is shown in Figure 4b. The adsorption capacity of PVAP for U(VI) increases with the increased temperature, which indicates that high temperature promotes the capture of U(VI) by PVKAP. The thermodynamic parameters of the adsorption process ( $\Delta H$ ), entropy change ( $\Delta S$ ), and Gibbs free energy change ( $\Delta G$ ) are listed in Table 3, and the details of the calculation Equations and methods are explained in the Supplementary Materials [47,48]. As shown in Table 3,  $\Delta G < 0$  indicates that the capturing of U(VI) by PVKAP is a spontaneous process. Furthermore, the absolute value of  $\Delta G$  increases with the increased temperature of the reaction system, which reveals that high temperature promotes the more efficiently capturing of U(VI) on PVKAP. In addition,  $\Delta H > 0$  reveals that the process of capturing U(VI) by PVKAP is an endothermic reaction; namely, increasing the temperature can increase the degree of reaction. This is also in accordance with the results of the adsorption isotherm experiment. Furthermore,  $\Delta S > 0$  reveals that the process is an entropy-driven adsorption process, which means the degree of freedom of the solid–liquid interface is increased after the capturing of U(VI) by PVKAP. Therefore, the efficient capturing of U(VI) by PVKAP is a spontaneous endothermic process.

**Table 3.** Thermodynamic parameters for U(VI) entrapment onto PVKAP.

Temperature (K)	$\Delta G^0$ (kJ mol <sup>-1</sup> )	$\Delta H^0$ (kJ mol <sup>-1</sup> )	$\Delta S^0$ (J mol <sup>-1</sup> K <sup>-1</sup> )
293	−11.75		
313	−15.53	43.57	188.72
333	−19.30		

### 3.4. Kinetics Study

Adsorption efficiency is a key factor in the overall performance evaluation of adsorbents in practical applications. Figure 5 shows that the capture rate of U(VI) by PVKAP is very fast and the adsorption equilibrium is reached within the contact time of 35 min (Figure 5a). For the purpose of further understanding the adsorption mechanism of U(VI) on PVKAP, a quasi-first-order kinetic model and a quasi-second-order kinetic model were used for fitting [49,50]. As shown in Table 4, the correlation coefficient ( $R^2$ ) of PVKAP for U(VI) adsorption fitting by quasi-second-order kinetics ( $R^2 = 0.994$ ) is higher than that of the quasi-first-order kinetic ( $R^2 = 0.980$ ), indicating the quasi-second-order kinetic model is more suitable to describing the adsorption process, thus, implying that the efficient capture of U(VI) by PVKAP mainly is attributable to surface complexation and the chemisorption of strong forces, rather than ion exchange [51,52]. Furthermore, the adsorption rate and capacity of U(VI) on PVKAP are significantly improved compared with PVK, which is mainly due to the abundant phosphonic acid groups and hydroxyl sites on the surface of PVKAP [39].

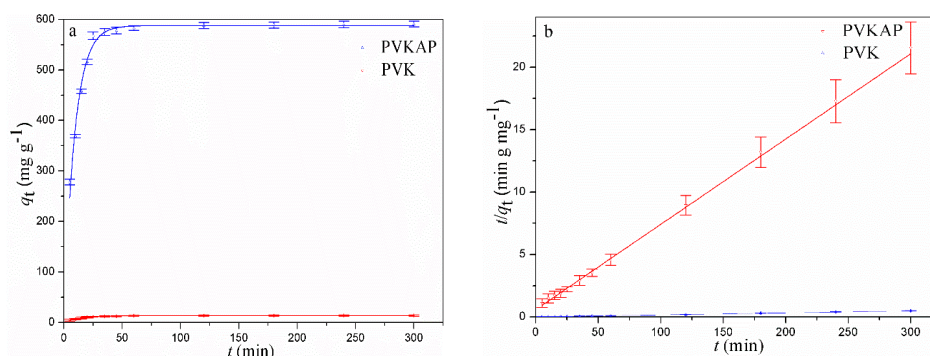


**Figure 5.** The influence of the adsorption reaction time of uranyl on PVK and PVKAP. (a) pseudo-first-order (b) pseudo-second-order.

**Table 4.** Parameters for pseudo-first-order and pseudo-second-order models.

Adsorbate	$K_1$ (min <sup>-1</sup> )	Pseudo-First-Order $q_e$ (mg g <sup>-1</sup> )	$R^2$	$K_2$ (g mg min <sup>-1</sup> )	Pseudo-Second-Order $q_e$ (mg g <sup>-1</sup> )	$R^2$
PVK	0.07	13.6	0.985	$7.92 \times 10^{-3}$	14.6	0.996
PVKAP	0.11	587.8	0.980	$2.72 \times 10^{-4}$	632.9	0.994

### 3.5. Influence of pH and Ionic Strength

The adsorption behavior of U(VI) is highly dependent on the pH of the solution (Figure 6), indicating that the adsorption of U(VI) by PVKAP is dominated by surface complexation [53]. These experiments were carried out under the condition of  $C_{U(VI)initial} = 36.0 \text{ mg L}^{-1}$ ,  $T = 293 \text{ K}$ , 11 different pH values (pH = 2, 3, 4, 5, 6, 7, 8, 9, 10, 11, 12, respectively) and three different ionic strengths (0.1 M NaNO<sub>3</sub>, 0.01 M NaNO<sub>3</sub>, 0.001 M NaNO<sub>3</sub>). When the pH value of the solution increased from 2.0 to 6.0, the removal rate of U(VI) by PVKAP increased from ~39.0% to ~96.2%, and then decreased to ~74.0% as the pH increased to 12.0. This result could be clarified by the intrinsic properties of the adsorbents and the speciation of U(VI) in the solution. When pH < 6, U(VI) is mainly present in solution in the form of  $UO_2^{2+}$ ,  $UO_2(OH)^+$  and  $(UO_2)_3(OH)^{5+}$  [54], the sharply increased removal rate of PVKAP could be attributed to the capture of  $UO_2^{2+}$  with a negatively charged active site on the surface of PVKAP. When pH > 6, the positively charged U(VI) speciation gradually decreases with the increased pH value, while the negatively charged speciation of U(VI) (e.g.,  $(UO_2)_3(OH)_7^-$ ) is gradually increased, thereby causing an increasing electrostatic repulsion between PVKAP and U(VI), and resulting in a decrease in the adsorption capacity [55–59].

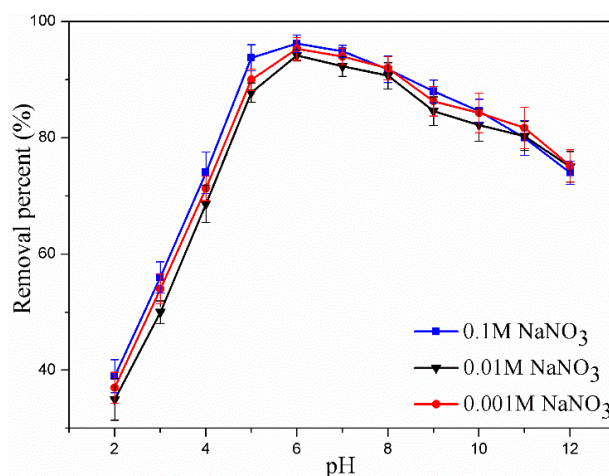


**Figure 6.** Influence of pH and ionic strength on the capturing U(VI) by PVKAP,  $C_{U(VI)initial} = 36.0 \text{ mg L}^{-1}$ ,  $T = 293 \text{ K}$ .

In addition, the adsorption behavior of PVKAP capturing U(VI) at different ionic strengths is shown in Figure 6. According to the reported literatures [29,60], the dependence of adsorption behavior on the ionic strength is an indirect method to distinguish the inner layer and the outer surface complexation. As shown in Figure 6, at the three ionic strengths (0.1 M NaNO<sub>3</sub>, 0.01 M NaNO<sub>3</sub>, 0.001 M NaNO<sub>3</sub>), the adsorption behavior of PVKAP is similar and there is no obvious adsorption boundary. Therefore, the inner layer complexation dominates the efficient capturing of U(VI) by PVKAP [29], which could be explained by the strong complexing ability of phosphonic acid groups and carboxyl groups on the surface of PVKAP.

### 3.6. Adsorption Selectivity and Recycling Performance Study

In consideration of the complexity and heterogeneity of the real aquatic environment, ICP-AES was adopted to check the adsorption selectivity of PVKAP versus U(VI) in a mixed solution containing Zr,

Cu, Eu, Co, Pb, Cr, U, Hg, Cd, La, Sr, Th, and Cs ( $C_0 = 0.5 \text{ mmol L}^{-1}$  for all these cations). As shown in Figure 7, PVKAP has significantly enhanced preferential affinity for uranyl compared to PVK, indicating that it is more capable of selectively enriching U(VI) from multi-component systems. According to Equation (3), the sorption selectivity ( $S_U$ ) of PVKAP to U(VI) is almost 70.36%, while PVK has almost no adsorption selectivity in the same condition. So, the excellent adsorption selectivity of PVKAP is mainly attributed to the excellent complexing ability between P = O group of PVKAP and U(VI). In addition, PVKAP shows a selective adsorption sequence: U(VI) > Eu(III)  $\approx$  La(III)  $\approx$  Th(IV) > other metal ions, which can be ascribed to the intrinsic properties of different metal ions and their affinity with PVKAP [61,62]. Moreover, the reusability of the adsorbent is an important performance of practical applications. Figure 8 shows the five recycling studies of PVK and PVKAP. The removal rate of U(VI) by PVK is reduced from 90% to 75%, while the removal rate of U(VI) by PVKAP is maintained above 96% (99% to 96%). Thus, it was shown that the PVKAP has largely improved recyclability.

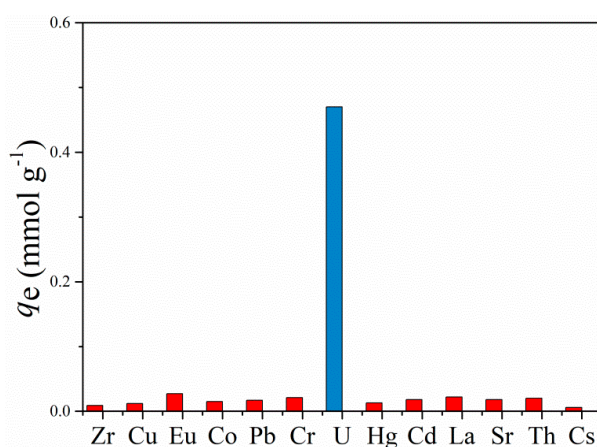


**Figure 7.** Competitive adsorption of coexistent ions by PVKAP,  $C_0 = 0.5 \text{ mmol L}^{-1}$  for all cations,  $\text{pH} = 5.0 \pm 0.1$ ,  $m/V = 0.05 \text{ g L}^{-1}$ .

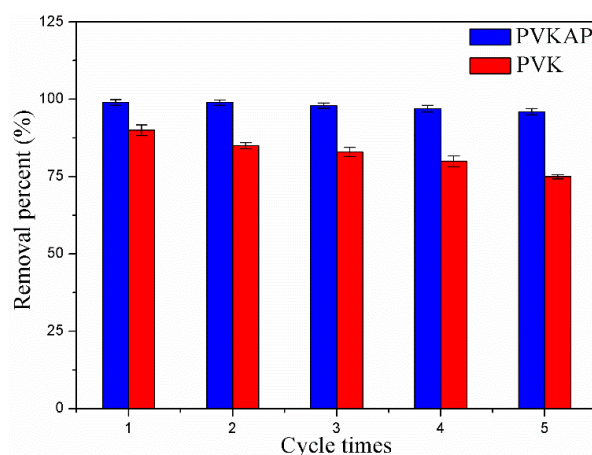


**Figure 8.** Reusability studies of PVK and PVKAP on the removal of U(VI) from aqueous solution,  $T = 293 \text{ K}$ ,  $\text{pH} = 5.0 \pm 0.1$ ,  $C_{\text{U(VI)initial}} = 36.0 \text{ mg L}^{-1}$ ,  $m/V = 0.1 \text{ g L}^{-1}$ .

### 3.7. Adsorption Mechanism

For the sake of further clarifying the adsorption mechanism of PVKAP to U(VI), XPS spectra were used to analyze the changes of surface functional groups after enrichment of U(VI) by PVKAP. Figure 9 shows that the specific enrichment of U(VI) by specific functional groups was deduced from the O 1s and P 2p fine XPS spectra of PVKAP. In general, there are two possible ways for the adsorption process between the phosphonic acid group and U(VI). One way is that the  $\text{H}^+$  of the phosphonic acid group is exchanged with U(VI) by ion-exchanged process, and the other way is by coordination

between the phosphonic acid group (P=O) and  $\text{UO}_2^{2+}$  [63]. The peaks at 134.05 (P 2p<sub>1/2</sub>) and 133.05 (P 2p<sub>3/2</sub>) eV shown in the P 2p high-resolution spectrum of PVKAP reveal that P 2p can be attributed to phosphorus atoms in two phosphine-containing groups.

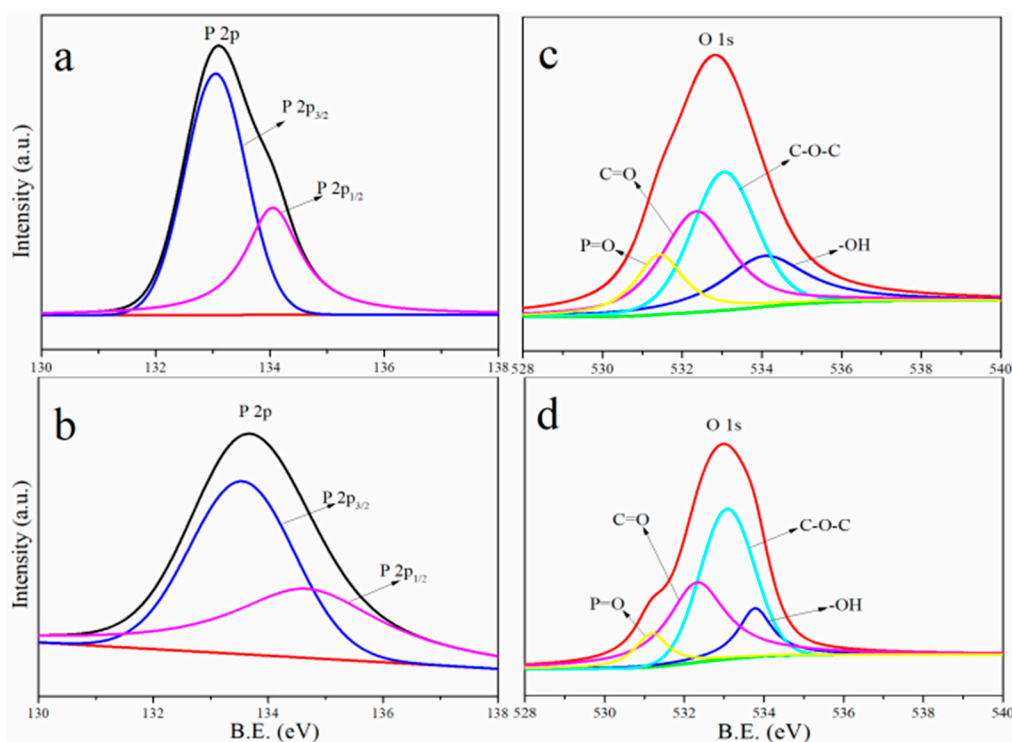


**Figure 9.** XPS spectra of P 2p for PVKAP before (a) and after (b) uranyl entrapment, O 1s for PVKAP before (c) and after (d) uranyl entrapment.

When PVKAP is loaded with U(VI), the peak intensities of P 2p<sub>3/2</sub> and P 2p<sub>1/2</sub> are significantly reduced, and the binding energies of P 2p<sub>3/2</sub> and P 2p<sub>1/2</sub> are increased from 133.05 and 134.05 eV to 133.55 and 134.65 eV, respectively. These results indicate that the phosphonic acid group forms a new chemical bond with  $\text{UO}_2^{2+}$  [41].

In addition, the O 1s high resolution spectrum from PVKAP can be divided into four peaks, namely peaks of 531.48, 532.38, 533.08, and 534.18 eV, respectively, corresponding to P=O, C=O, C-O-C, and -OH [11,64]. When the PVKAP is loaded with U(VI), the characteristic peaks at P=O and -OH move from 531.48 and 534.18 eV to 531.18 and 533.78 eV, respectively, and the relative peak area decreases significantly, indicating a coordination of P=O and -OH with U(VI) was formed. However, after PVKAP loading with U(VI), the positions of the peaks for C-O-C and C=O remained unchanged, indicating that C-O-C and C=O did not participate in the coordination. Therefore, the enrichment of U(VI) by PVKAP can be mainly ascribed to the coordination of phosphonic acid groups rather than carboxyl sites.

#### 4. Conclusions

In this study, a novel phosphonic acid functionalized cellulose adsorbent (PVKAP) with a simple preparation route is used for the highly efficient and selective adsorption of U(VI). The effects of different temperatures, contact times, pH values, ionic strengths, and competitive adsorptions of various metal ions were studied to explore the adsorption mechanism of the prepared adsorption materials to U(VI). The adsorption behavior conforms to the Langmuir adsorption model and the pseudo-second-order kinetics model. Owing to the strong coordination between phosphonic acid groups and U(VI), the adsorption performance of PVKAP is obviously higher than that of PVK. The maximum adsorption capacities (pH = 5,  $T = 293$  K) of PVK and PVKAP based on Langmuir

isotherm model are 57.2 and 714.3 mg g<sup>-1</sup>, and the adsorption equilibrium reaches in 240 and 35 min, indicating that PVKAP has great potential value to capture U (VI). Moreover, PVKAP has high adsorption selectivity for U(VI) (sorption selectivity is 70.36%) and good recyclability. The results of batch adsorption experiments and spectral analysis reveal that the efficient capture of U(VI) by PVKAP is mainly regulated by the inner layer complexation. Given the environmental friendliness of PVKAP, its ease of preparation, and low cost, it has good application potential value for U(VI) enrichment in aqueous media related to nuclear waste.

**Supplementary Materials:** The following are available online at <http://www.mdpi.com/2076-3417/10/16/5455/s1>, Figure S1: Schematic of the synthetic route of PVKAP, Figure S2: Original data for XPS experiments.

**Author Contributions:** Conceptualization, Z.H.; Funding acquisition, Z.H., H.Z. and J.L.; Investigation, Z.H., S.Z. and J.Y.; Project administration, Z.H. and J.L.; Supervision, H.Z.; Validation, S.Z. and J.Y.; Writing—original draft, Z.H., S.Z. and J.Y.; Writing—review and editing, Z.H. and J.L. All authors have read and agreed to the published version of the manuscript.

**Funding:** This research received no external funding.

**Acknowledgments:** The work was financially supported by the National Natural Science Foundation of China (Nos. 21677146, 21777165, 21876178), and the Anhui Provincial Natural Science Foundation (No. 1708085MB31).

**Conflicts of Interest:** The authors declare no conflict of interest.

## References

1. Craft, E.S.; Abuqare, A.W.; Flaherty, M.M.; Garofolo, M.C.; Rincavage, H.L.; Abouondonia, M.B. Depleted and natural uranium: Chemistry and toxicological effects. *J. Toxicol. Environ. Health B* **2004**, *7*, 297–317. [[CrossRef](#)]
2. O’Loughlin, E.J.; Kelly, S.D.; Cook, R.E.; Csencsits, R.; Kemner, K.M. Reduction of uranium (VI) by mixed iron(II)/iron(III) hydroxide (green rust): Formation of UO<sub>2</sub> nanoparticles. *Environ. Sci. Technol.* **2003**, *37*, 721–727. [[CrossRef](#)]
3. Camacho, L.M.; Deng, S.; Parra, R.R. Uranium removal from groundwater by natural clinoptilolite zeolite: Effects of pH and initial feed concentration. *J. Hazard. Mater.* **2010**, *189*, 286–293. [[CrossRef](#)]
4. Mori, T.; Takao, K.; Sasaki, K.; Suzuki, T.; Arai, T.; Ikeda, Y. Homogeneous liquid–liquid extraction of U(VI) from HNO<sub>3</sub> aqueous solution to betainium bis(trifluoromethylsulfonyl)imide ionic liquid and recovery of extracted U(VI). *Sep. Purif. Technol.* **2015**, *155*, 133–138. [[CrossRef](#)]
5. Zhang, S.; Zhao, X.; Li, B.; Bai, C.; Li, Y.; Wang, L.; Wen, R.; Zhang, M.; Ma, L.; Li, S. “Stereoscopic” 2D super-microporous phosphazene-based covalent organic framework: Design, synthesis and selective sorption towards uranium at high acidic condition. *J. Hazard. Mater.* **2016**, *314*, 95–104. [[CrossRef](#)] [[PubMed](#)]
6. Popescu, I.C.; Filip, P.; Humelnicu, D.; Humelnicu, I.; Scott, T.B.; Crane, R.A. Removal of uranium(VI) from aqueous systems by nanoscale zero-valent iron particles suspended in carboxy-methyl cellulose. *J. Nucl. Mater.* **2013**, *443*, 250–255. [[CrossRef](#)]
7. Yang, C.T.; Pei, S.Q.; Chen, B.H.; Ye, L.N.; Yu, H.Z.; Hu, S. Density functional theory investigations on the binding modes of amidoximes with uranyl ions. *Dalton Trans.* **2016**, *45*, 3120–3129. [[CrossRef](#)] [[PubMed](#)]
8. Wang, Y.; Chen, Y.; Liu, C.; Yu, F. Preparation of porous magnesium oxide foam and study on its enrichment of uranium. *J. Nucl. Mater.* **2018**, *504*, 166–175. [[CrossRef](#)]
9. Vanengelen, M.R.; Szilagyi, R.K.; Gerlach, R.; Lee, B.D.; Apel, W.A.; Peyton, B.M. Uranium exerts acute toxicity by binding to pyrroloquinoline quinone cofactor. *Environ. Sci. Technol.* **2011**, *45*, 937–942. [[CrossRef](#)]
10. Trenfield, M.A.; Ng, J.C.; Noller, B.N.; Markich, S.J.; Dam, R.A.V. Dissolved organic carbon reduces uranium bioavailability and toxicity. 2. Uranium(VI) speciation and toxicity to three tropical freshwater organisms. *Environ. Sci. Technol.* **2011**, *45*, 3082–3089. [[CrossRef](#)]
11. Shao, D.; Hou, G.; Li, J.; Tao, W.; Ren, X.; Wang, X. PANI/GO as a super adsorbent for the selective adsorption of uranium(VI). *Chem. Eng. J.* **2014**, *255*, 604–612. [[CrossRef](#)]
12. Lv, K.; Han, J.; Yang, C.T.; Cheng, C.M.; Luo, Y.M.; Wang, X.L. A category of hierarchically porous tin (IV) phosphonate backbone with the implication for radioanalytical separation. *Chem. Eng. J.* **2016**, *302*, 368–376. [[CrossRef](#)]

13. Jang, J.H.; Dempsey, B.A.; Burgos, W.D. A model-based evaluation of sorptive reactivities of hydrous ferric oxide and hematite for U(VI). *Environ. Sci. Technol.* **2007**, *41*, 4305–4310. [[CrossRef](#)] [[PubMed](#)]
14. Tolkou, A.K.; Katsoyiannis, I.A.; Zouboulis, A.I. Removal of arsenic, chromium and uranium from water sources by novel nanostructured materials including graphene-based modified adsorbents: A mini review of recent developments. *Appl. Sci.* **2020**, *10*, 3241. [[CrossRef](#)]
15. Han, B.; Zhang, E.; Cheng, G. Facile preparation of graphene oxide-MIL-101(Fe) composite for the efficient capture of uranium. *Appl. Sci.* **2018**, *8*, 2270. [[CrossRef](#)]
16. Ling, L.W.; Feng, L.; Li, L.D.; Jian, Q.L.; Xiao, L.W.; Shu, J.L.; Ming, B.L. Ultrafast high-performance extraction of uranium from seawater without pretreatment using an acylamide- and carboxyl-functionalized metal–organic framework. *J. Mater. Chem. A* **2015**, *3*, 13724–13730.
17. Yang, W.; Bai, Z.; Shi, W.; Yuan, L.; Tian, T.; Chai, Z.; Wang, H.; Sun, Z. MOF-76: From a luminescent probe to highly efficient U–VI sorption material. *Chem. Commun.* **2013**, *49*, 10415–10417. [[CrossRef](#)]
18. Carboni, M.; Abney, C.W.; Liu, S.; Lin, W. Highly porous and stable metal–organic frameworks for uranium extraction. *Chem. Sci.* **2013**, *4*, 2396–2402. [[CrossRef](#)]
19. Yuan, G.Y.; Tu, H.; Liu, J.; Zhao, C.S.; Liao, J.L.; Yang, Y.Y.; Yang, J.J.; Liu, N. A novel ion-imprinted polymer induced by the glycyglycine modified metalorganic framework for the selective removal of Co (II) from aqueous solutions. *Chem. Eng. J.* **2018**, *333*, 280–288. [[CrossRef](#)]
20. Zhao, D.; Feng, J.; Huo, Q.; Melosh, N.; Fredrickson, G.H.; Chmelka, B.F.; Stucky, G.D. Triblock copolymer syntheses of mesoporous silica with periodic 50 to 300 Angstrom Pores. *Science* **1998**, *279*, 548–552. [[CrossRef](#)]
21. Zhang, W.; Ye, G.; Chen, J. Study on the gamma-ray irradiation behavior of mesoporous silica adsorbents functionalized with phosphine oxide and phosphonic acid ligands. *J. Radioanal. Nucl. Chem.* **2016**, *307*, 1445–1451. [[CrossRef](#)]
22. Lebed, P.J.; De, S.K.; Bilodeau, F.; Larivière, D.; Kleitz, F. Phosphonate-functionalized large pore 3-D cubic mesoporous (KIT-6) hybrid as highly efficient actinide extracting agent. *Chem. Commun.* **2011**, *47*, 11525–11527. [[CrossRef](#)] [[PubMed](#)]
23. Li, F.; Yang, J.; Liao, J.; Li, S.; Liao, J.; Prabhu, R.; Williams, L.N.; Yang, Y.; Tang, J.; Ning, L. Direct synthesis of carbon-based microtubes by hydrothermal carbonization of microorganism cells. *Chem. Eng. J.* **2015**, *276*, 322–330. [[CrossRef](#)]
24. Fafous, I.I.; Dawoud, J.N. Uranium (VI) sorption by multiwalled carbon nanotubes from aqueous solution. *Appl. Surf. Sci.* **2012**, *259*, 433–440. [[CrossRef](#)]
25. Deb, A.K.S.; Ilaiyaraja, P.; Ponraju, D.; Venkatraman, B. Diglycolamide functionalized multi-walled carbon nanotubes for removal of uranium from aqueous solution by adsorption. *J. Radioanal. Nucl. Chem.* **2012**, *291*, 877–883. [[CrossRef](#)]
26. Bing, H.; Zhang, E.; Gong, C.; Zhang, L.; Wang, D.; Wang, X. Hydrothermal carbon superstructures enriched with carboxyl groups for highly efficient uranium removal. *Chem. Eng. J.* **2018**, *338*, 734–744.
27. Hokkanen, S.; Bhatnagar, A.; Sillanpää, M. A review on modification methods to cellulose-based adsorbents to improve adsorption capacity. *Water Res.* **2016**, *91*, 156–173.
28. Han, X.; Xu, M.; Yang, S.; Qian, J.; Hua, D. Acetylcysteine-functionalized microporous conjugated polymers for potential separation of uranium from radioactive effluents. *J. Mater. Chem. A* **2017**, *5*, 5123–5128. [[CrossRef](#)]
29. Yuan, D.; Chen, L.; Xiong, X.; Yuan, L.; Liao, S.; Wang, Y. Removal of uranium (VI) from aqueous solution by amidoxime functionalized superparamagnetic polymer microspheres prepared by a controlled radical polymerization in the presence of DPE. *Chem. Eng. J.* **2016**, *285*, 358–367. [[CrossRef](#)]
30. Bhatnagar, A.; Sillanpää, M.; Witekrowiak, A. Agricultural waste peels as versatile biomass for water purification—A review. *Chem. Eng. J.* **2015**, *270*, 244–271. [[CrossRef](#)]
31. Mohammed, N.; Grishkewich, N.; Berry, R.; Tam, K. Cellulose nanocrystal-alginate hydrogel beads as novel adsorbents for organic dyes in aqueous solutions. *Cellulose* **2015**, *22*, 3725–3738. [[CrossRef](#)]
32. Wei, H.; Rodriguez, K.; Renneckar, S.; Vikesland, P.J. Environmental science and engineering applications of nanocellulose-based nanocomposites. *Environ. Sci. Nano* **2014**, *1*, 302–316. [[CrossRef](#)]
33. Faruk, O.; Bledzki, A.K.; Fink, H.; Sain, M. Biocomposites reinforced with natural fibers: 2000–2010. *Prog. Polym. Sci.* **2012**, *37*, 1552–1596. [[CrossRef](#)]
34. Henriksson, M.; Berglund, L. Structure and properties of cellulose nanocomposite films containing melamine formaldehyde. *J. Appl. Polym. Sci.* **2007**, *106*, 2817–2824. [[CrossRef](#)]

35. O'Connell, D.W.; Birkinshaw, C.; O'Dwyer, T.F. Heavy metal adsorbents prepared from the modification of cellulose: A review. *Bioresour. Technol.* **2008**, *99*, 6709–6724. [[CrossRef](#)]
36. Bayramoglu, G.; Altintas, B.; Arica, M.Y. Synthesis and characterization of magnetic beads containing aminated fibrous surfaces for removal of Reactive Green 19 dye: Kinetics and thermodynamic parameters. *J. Chem. Technol. Biotechnol.* **2012**, *87*, 705–713. [[CrossRef](#)]
37. Anirudhan, T.S.; Nima, J.; Divya, P.L. Adsorption of chromium(VI) from aqueous solutions by glycidylmethacrylate-grafted-densified cellulose with quaternary ammonium groups. *Appl. Surf. Sci.* **2013**, *279*, 441–449. [[CrossRef](#)]
38. Yang, J.; Kubota, F.; Baba, Y.; Kamiya, N.; Goto, M. Application of cellulose acetate to the selective adsorption and recovery of Au(III). *Carbohydr. Polym.* **2014**, *111*, 768–774. [[CrossRef](#)]
39. Cai, Y.; Wu, C.; Liu, Z.; Zhang, L.; Chen, L.; Wang, J.; Wang, X.; Yang, S.; Wang, S. Fabrication of a phosphorylated graphene oxide–chitosan composite for highly effective and selective capture of U(VI). *Environ. Sci. Nano* **2017**, *4*, 1876–1886. [[CrossRef](#)]
40. Yi, J.; Huo, Z.; Tan, X.; Chen, C.; Asiri, A.M.; Alamry, K.A.; Li, J. Plasma-facilitated modification of pumpkin vine-based biochar and its application for efficient elimination of uranyl from aqueous solution. *Plasma Sci. Technol.* **2019**, *21*, 095502. [[CrossRef](#)]
41. Yuan, D.; Yun, W.; Yong, Q.; Yan, L.; Gang, F.; Huang, B.; Zhao, X. Highly selective adsorption for uranium in strong HNO<sub>3</sub> media achieved on phosphonic acid functionalized nanoporous polymer. *J. Mater. Chem. A* **2017**, *5*, 22735–22742. [[CrossRef](#)]
42. Zhao, G.; Li, J.; Ren, X.; Chen, C.; Wang, X. Few-Layered Graphene Oxide Nanosheets As Superior Sorbents for Heavy Metal Ion Pollution Management. *Environ. Sci. Technol.* **2011**, *45*, 10454–10462. [[CrossRef](#)] [[PubMed](#)]
43. Gentilhomme, A.; Cochez, M.; Ferriol, M.; Oget, N.; Mieloszynski, J.L. Thermal degradation of methyl methacrylate polymers functionalized by phosphorus-containing molecules—II: Initial flame retardance and mechanistic studies. *Polym. Degrad. Stab.* **2003**, *82*, 347–355. [[CrossRef](#)]
44. Goods, J.B.; Sydlik, S.A.; Walish, J.J.; Swager, T.M. Phosphate functionalized graphene with tunable mechanical properties. *Adv. Mater.* **2014**, *26*, 718–723. [[CrossRef](#)]
45. Chen, C.; Yu, Y.; Wei, L.; Cao, C.; Ping, L.; Dou, Z.; Song, W. Mesoporous Ce<sub>1-x</sub>Zr<sub>x</sub>O<sub>2</sub> solid solution nanofibers as high efficiency catalysts for the catalytic combustion of VOCs. *J. Mater. Chem.* **2011**, *21*, 12836–12841. [[CrossRef](#)]
46. Crea, J.; DiGiusto, R.; Lincoln, S.F.; Williams, E.H. A nuclear magnetic resonance study of ligand exchange on dioxopentakis(trimethyl phosphate)uranium(VI) ion and its triethyl phosphate analog. *Inorg. Chem.* **1977**, *16*, 2825–2829. [[CrossRef](#)]
47. Lyubchik, S.I.; Lyubchik, A.I.; Galushko, O.L.; Tikhonova, L.P.; Vital, J.; Fonseca, I.M.; Lyubchik, S.B. Kinetics and thermodynamics of the Cr(III) adsorption on the activated carbon from co-mingled wastes. *Colloids Surfaces A* **2004**, *242*, 151–158. [[CrossRef](#)]
48. Zhao, G.; Zhang, H.; Fan, Q.; Ren, X.; Li, J.; Chen, Y.; Wang, X. Sorption of copper(II) onto super-adsorbent of bentonite–polyacrylamide composites. *J. Hazard. Mater.* **2010**, *173*, 661–668. [[CrossRef](#)]
49. Corbett, J.F. Pseudo first-order kinetics. *J. Chem. Educ.* **1972**, *49*, 663. [[CrossRef](#)]
50. Ho, Y.S.; McKay, G. A comparison of chemisorption kinetic models applied to pollutant removal on various sorbents. *Process. Saf. Environ.* **1998**, *76*, 332–340. [[CrossRef](#)]
51. Ho, Y.S.; McKay, G. The kinetics of sorption of divalent metal ions onto sphagnum moss peat. *Water Res.* **2000**, *34*, 735–742. [[CrossRef](#)]
52. Song, X.; Gunawan, P.; Jiang, R.; Leong, S.S.; Wang, K.; Xu, R. Surface activated carbon nanospheres for fast adsorption of silver ions from aqueous solutions. *J. Hazard. Mater.* **2011**, *194*, 162–168. [[CrossRef](#)] [[PubMed](#)]
53. Maneerung, T.; Liew, J.; Dai, Y.J.; Kawi, S.; Chong, C.; Wang, C.H. Activated carbon derived from carbon residue from biomass gasification and its application for dye adsorption: Kinetics, isotherms and thermodynamic studies. *Bioresour. Technol.* **2015**, *200*, 350–359. [[CrossRef](#)]
54. Yang, S.; Zong, P.; Hu, J.; Sheng, G.; Qi, W.; Wang, X. Fabrication of  $\beta$ -cyclodextrin conjugated magnetic HNT/iron oxide composite for high-efficient decontamination of U(VI). *Chem. Eng. J.* **2013**, *214*, 376–385. [[CrossRef](#)]
55. Tokunaga, T.K.; Kim, Y.; Wan, J.; Yang, L. Aqueous uranium(VI) concentrations controlled by calcium uranyl vanadate precipitates. *Environ. Sci. Technol.* **2012**, *46*, 7471–7477. [[CrossRef](#)] [[PubMed](#)]

56. Madadrang, C.J.; Kim, H.Y.; Gao, G.; Ning, W.; Zhu, J.; Feng, H.; Gorring, M.; Kasner, M.L.; Hou, S. Adsorption behavior of EDTA-graphene oxide for Pb (II) removal. *ACS Appl. Mater. Interfaces* **2012**, *4*, 1186–1193. [[CrossRef](#)]
57. Hayes, F.K.; Leckie, O.J. Modeling ionic strength effects on anion adsorption at hydrous oxide/solution interfaces. *J. Colloid Interface Sci.* **1987**, *115*, 564–572. [[CrossRef](#)]
58. Volkov, A.G.; Paula, S.; Deamer, D.W. Two mechanisms of permeation of small neutral molecules and hydrated ions across phospholipid bilayers. *Bioelectroch. Bioenerg.* **1997**, *42*, 153–160. [[CrossRef](#)]
59. Jin, Z.; Wang, X.; Sun, Y.; Ai, Y.; Wang, X. Adsorption of 4-n-Nonylphenol and Bisphenol-A on Magnetic Reduced Graphene Oxides: A Combined Experimental and Theoretical Studies. *Environ. Sci. Technol.* **2015**, *49*, 9168–9175. [[CrossRef](#)]
60. Li, F.Z.; Li, D.M.; Li, X.L.; Liao, J.L.; Li, S.J.; Yang, J.J.; Yang, Y.Y.; Tang, J.; Liu, N. Microorganism-derived carbon microspheres for uranium removal from aqueous solution. *Chem. Eng. J.* **2016**, *284*, 630–639. [[CrossRef](#)]
61. Li, N.; Zhang, L.; Chen, Y.; Fang, M.; Zhang, J.; Wang, H. Highly Efficient, Irreversible and Selective Ion Exchange Property of Layered Titanate Nanostructures. *Adv. Funct. Mater.* **2012**, *22*, 835–841. [[CrossRef](#)]
62. De Smet, F.; Ruiz, P.; Delmon, B.; Devillers, M. Rationalization of the Catalytic Behavior of Lanthanide Oxides and Praseodymium Molybdates in Total and Selective Oxidation of Isobutene. *J. Phys. Chem. B* **2001**, *105*, 12355–12363. [[CrossRef](#)]
63. Venkatesan, K.A.; Shyamala, K.V.; Antony, M.P.; Srinivasan, T.G.; Rao, P.R.V. Batch and dynamic extraction of uranium(VI) from nitric acid medium by commercial phosphinic acid resin, Tulsion CH-96. *J. Radioanal. Nucl. Chem.* **2008**, *275*, 563–570. [[CrossRef](#)]
64. Amaral, I.F.; Granja, P.L.; Barbosa, M.A. Chemical modification of chitosan by phosphorylation: An XPS, FT-IR and SEM study. *J. Biomater. Sci. Polym. Ed.* **2005**, *16*, 1575–1593. [[CrossRef](#)]



© 2020 by the authors. Licensee MDPI, Basel, Switzerland. This article is an open access article distributed under the terms and conditions of the Creative Commons Attribution (CC BY) license (<http://creativecommons.org/licenses/by/4.0/>).